Testing and Optimization of High Q-Factor Magnetoelectric Devices

Ann Bonde (University of Minnesota, BMEn and CS), $SUNFESTFellow$
Sydney Sofronici, ESE
Dr. Troy Olsson, ESE

***Abstract*— Biomagnetic sensing requires not only high device sensitivity, but also a large bandwidth (∼1kHz). MEMS devices utilizing magnetostrictive and piezoelectric materials show promise in these applications. Additionally, a low frequency feature of these devices allows for use in Wireless Power Transfer (WPT) applications. Optimal performance is achieved by driving the device at resonance under a DC magnetic bias field. Here, a testing configuration was designed and assembled to accommodate these features. To maximize Signal to Noise Ratio (SNR), the DC bias field was tested at various magnitudes and angles. A system of two sets of electromagnetic coils were arranged orthogonally to achieve a rotating DC field. SNR and Q-factor data from the device is reported for the higher (∼6.5 MHz) and lower (∼80kHz) frequency modes in varied DC bias fields. Future steps include integrating permanent magnets at the appropriate angle into the device board design as well as the use of Hall magnetic sensors to continuously characterize this bias field.**

***Index Terms*— MEMS, Multiferroics, Magnetometers, Biomagnetic Sensing, Modulation, Wireless Power Transfer, DC Magnetic Biasing**

I. INTRODUCTION

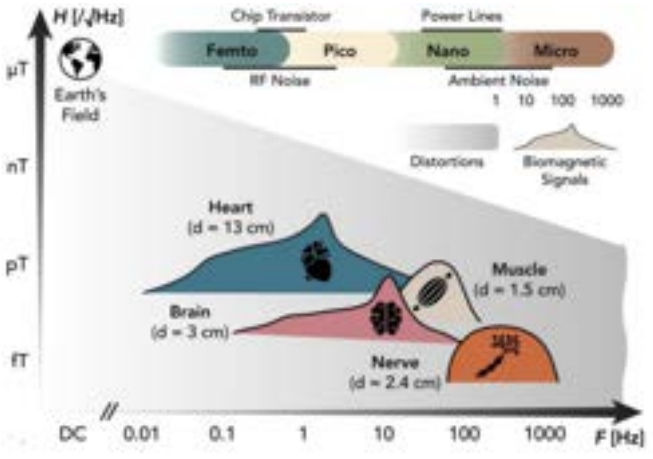

Fig. 1: Biomagnetic signal amplitude and frequency ranges [2].

Micro-electromechanical systems (MEMS) offer high performance devices at small sizes leading to a variety of applications in both consumer and industrial products. Specifically, in the field of biomedical engineering, these devices have the capability to detect small magnetic fields over a large bandwidth (>1 kHz) [1]. In addition to a range of frequencies, these signals are challenging to capture due to variation in amplitude from low femto-Teslas in the nervous system to hundreds of pico-Teslas in the heart. The Earth's magnetic field is roughly six orders of magnitude larger, imposing a high sensitivity requirement. Current techniques for biomagnetic measurements utilize sensitive Superconducting QUantum Interference Devices (SQUIDs) for magnetoencephalography (MEG) [3]. These systems require an expensive liquid helium cooling process that leads to issues with temperature isolation, making the technology less accessible.

Additionally, biomedical implants rely on MEMS devices for wireless power transfer (WPT). Current solutions, based around coupled resonant coils, show high power transfer efficiency but low quality factors (Q-factor) impose a trade-off between range of use and footprint sizes [4]. There is a need for a new method of providing power at longer ranges, with smaller footprints, while maintaining efficacy.

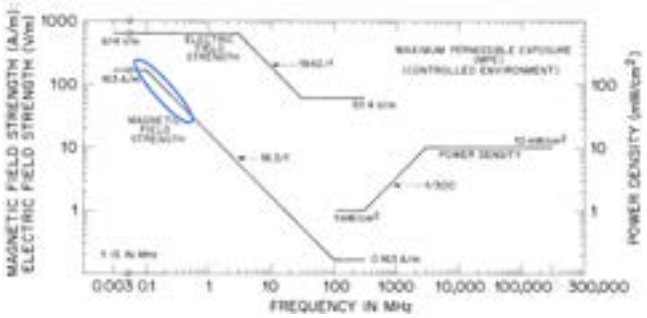

Fig. 2: IEEE Safety Standards for Human Exposure to EM Fields [6].

Magnetoelectric MEMS devices offer advantages in both sensing and WPT applications. Magnetoelectric (ME) sensors are shown to have a small footprint, low weight, and low power consumption. These devices take advantage of magnetostrictive and piezoelectric material properties to convert magnetic signals into current outputs. A key advantage to SQUID sensors is the capability of ME devices to operate at room temperature while maintaining comparable sensitivity levels [5]. In WPT applications, ME devices allow for higher Q-factors as compared to coupled coil systems [7]. The device has the ability to operate in low frequency ranges, shown in blue in Figure 2, allowing high power transmission. These devices have the potential to be used in both biomagnetic sensing and WPT applications making them a key advancement for implantable devices.

ME devices studied in this paper are composed of both a magnetostrictive (MS) layer of FeCo and a piezoelectric

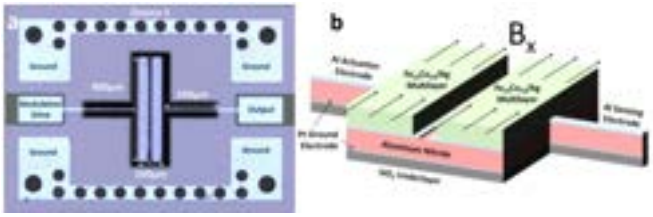

Fig. 3: ME device image (a) and layered beam schematic (b) [1].

(PE) layer of AlScN alloy. An image of the layered magnetoelectric device is shown in Figure 3 along with ground and sensing pads. In this ski design, one side of the beam acts as an actuating electrode while the other acts as a sensing electrode. There are two functions of the device studied here; the first being a high frequency mode and the second being a low frequency mode. When modulated to a resonant frequency of approximately 6.5 MHz, a high Qfactor (>1000 in some devices) leads to sensitive signal readings with low noise [1]. In this mode the beam extends and compresses along the neural axis. Biomagnetic sensing is feasible in this mode of operation due to the high sensitivity. Additionally, a bending resonance occurs when the device is exposed to signals of 70 kHz. Rather than extending as it does in the higher frequency range, the neutral axis strains in a fluctuating U-shape. The Q-factor in the lower frequency regime is not large enough to detect small external signals, but is large enough to efficiently transfer power from the resonant magnetic signal. This low frequency puts the device within range for high powered WPT that is safe for the human body [6].

II. BACKGROUND

A. Magnetoelectric (ME) Effect

Magnetostrictive (MS) materials are characterized by the production of material strain when exposed to a change in external magnetic field. Molecular magnetic dipoles rotate to align with the signal. Entire magnetic domains within the material experience this and orient to align with changes in the field, producing deformations in the material as a whole [8].

Piezoelectric (PE) materials produce a charge differential when exposed to stress. This phenomenon is due to the atomic crystal structure elongating or compressing from the applied stress. The charge distribution becomes asymmetrical in the unit cell, causing a polarization to appear in the direction of the force. This occurs throughout the bulk of the material, causing a net voltage change to occur across the sample [9].

When mechanically coupled, the multiferroic properties of the layers act to convert magnetic signal inputs to current outputs. Magnetic signals strain the MS layer, causing the coupled PE layer to strain and produce a voltage change [8, 9]. In the device here, an Iron Cobalt layer provides magnetostriction while an Aluminum-Scandium-Nitride layer provides the piezoelectric effect. Together the layers strain and output current can be detected from the sensing electrode via a thin tether. The ME effect refers to the device's ability to strain in response to magnetic signals. A greater ME effect indicates higher response with lower input.

B. Electrical Testing

ME devices here are first characterized using electrical testing. This is conducted using a vector network analyzer (VNA) to verify the piezoelectric property of the device. This machine sends electrical signals to the beam in a frequency sweep. A signal at a known power is sent in one side of the device via the tether from one channel of the VNA. Either the reflected signal can be measured on the same channel for an S11 measurement, or, the through-signal can be obtained from the other channel for an S21 measurement. The scattering parameters from an S21 measurement are used most frequently here. A functioning device will strain a maximum amount at its resonant frequency, causing low impedance and, therefore, a sharp peak on the VNA output. From this peak, the mechanical Q-factor of the device is obtained as shown in the example S21 measurement in Figure 4.

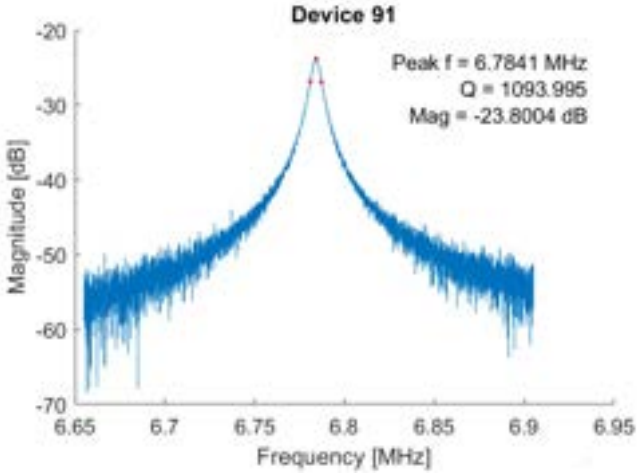

Fig. 4: Example S21 VNA plot for ski device in higher frequency mode.

Ski devices show the highest electrical response in the higher frequency mode at a resonance of around 6.5 MHz. Devices that operate well in the lower frequency mode also exhibit a lower frequency peak on the VNA. This occurs around 80kHz where the beam is in the bending mode, as opposed to extensional strain. Resonant frequencies determined during electrical testing are then used to test and optimize device performance in subsequent tests.

C. Magnetic Testing

To test the overall ability to capture magnetic signals, the device is exposed to an AC magnetic field that is tuned to the resonant frequency. Maximal strain in this AC field occurs when the MS material is biased with a DC magnetic field. In previous studies, the magnitude of DC bias magnitude was swept to determine the optimal level. At each magnitude,

the Young's modulus of the device changes slightly as a result of the changes in material stress; to accommodate this, the resonant frequency produced by the AC signal generator is adjusted to find a new resonant frequency that produces maximum response.

Bias that produces the highest power level from the device at the new resonance can then be used to report final sensing and WPT capabilities. Identifying the lower frequency resonance and bias correlated to highest levels of device bending provides insight into the full WPT capability of the device. For the sensing mode of the device, a modulation technique is used to detect fields similar to biomagnetic signals. Both of these final applications require that the optimal bias field be found using magnetic testing.

D. DC Magnetic Biasing

As mentioned, effective response requires that the dipoles of the magnetostrictive material are oriented in a way that produces maximum strain [10]. This is accomplished by exposing the device to a DC magnetic bias field. In an ideal device for sensing and WPT, it is desired to have a maximum change in strain from a minimum change in signal; in other words, a high device sensitivity. The magnetoelectric coefficient, represents the relationship of the stress curve derivative with respect to field level. Figure 5 represents how this slope impacts the output of an ME device. The red unbiased input has a large magnitude, but since the slope of the strain response is very small, the output strain is not significant. Conversely, the small biased input shown in blue is amplified by the large slope that occurs when the material is biased. Biasing the material with a DC field allows the device to operate at this point, where the slope of the magnetostriction curve (ME coefficient) is at a maximum.

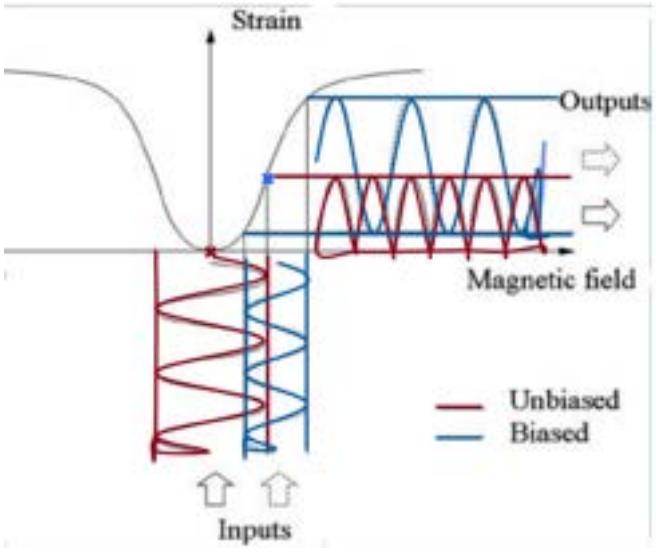

Fig. 5: Magnetostriction curve with sample comparison of unbiased and biased input signals [10].

However, total strain of a magnetostrictive material has shown dependence on bias field angle as well as magnitude [11]. This effect varies by MS material, but the overall impact on ME devices is virtually unexplored. Thus, optimization of the bias field angle has potential to improve the ME effect and device performance [8]. Studies have shown that when the AC and DC components of the external field are orthogonal to each other, a MS ribbon centered in the fields can experience maximal strain at a non-zero angle max relative to the horizontal [12]. This was tested for maximizing the second harmonic resonance in particular.

Building on these findings, an angled DC bias field will alter magnetostriction behavior allowing a maximum sensitivity to be found for both modes of device operation. This effective DC bias can be quantified at an angle, eff , relative to the longitudinal axis of the device. If the field magnitude is kept constant at the level found in magnetic testing, only the dipole orientation will change, maintaining the strain magnitude experienced at the neutral axis of the device [12]. Therefore starting at a low magnitude and sweeping different angles before increasing the magnitude and repeating the process will ensure a complete insight into the device behavior.

III. Methods

Here, the novel testing design is presented. Shown in Figure 6 is the CAD components of the design generated using SOLIDWORKS. The device is wire bonded to a PCB board and sits in the center of the DC bias coils and AC signal coils. Output voltage goes from the device and amplifier boards to a VNA or spectrum analyzer to capture electrical and magnetic responses respectively. Specific details on the purpose and technical aspects of the testing design are outlined.

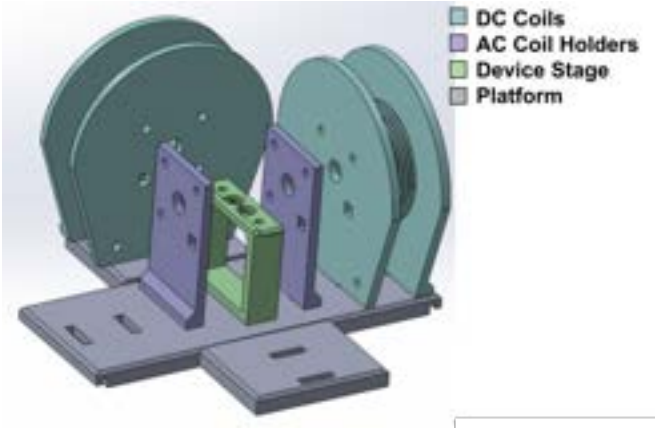

Fig. 6: Redesigned testing structure for angled DC bias and general testing.

A. DC Bias Coils

To provide a DC magnetic bias at an angle, two sets of Helmholtz coils were designed. These four total coils were designed to work together to generate an experienced angled field at the center. Figure 7 shows a schematic view of how the combined field method works. Since magnetic field behave as vectors in that the direction and magnitude obey

linear addition, these parallel and perpendicular components combine to generate a magnitude of Beff at angle eff.

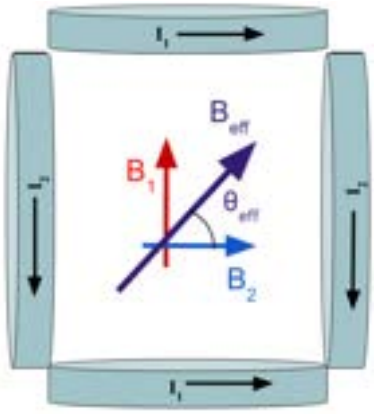

Fig. 7: Schematic of angled DC bias coil configuration.

Each coil set was designed to generate approximately 16mT with 5A of current in a true Helmholtz arrangement. Each coil has 125 turns of 14 AWG wire, yielding a combined resistance of 0.72Ω when in series. Since magnetic field falls off with 1d3 as distance d increases between the coils, the actual experienced field at the center becomes closer to 2.5 mT at 5A in the square configuration shown. In addition to the ability to generate an angled bias field between 0 - 2.5 mT, the DC coil structures also have spaces to directly attach the AC signal generating coils, allowing for compact testing.

Characterizing the field levels from these coils was done using a DC magnetic probe. Each coil set was investigated separately and then verified in the arrangement shown in Figure 7. Separately, the coils were subjected to an increasing current and the resulting field level in the center was recorded. This provides a linear relationship between magnetic field and current from which a constant slope coefficient is attained. Using basic trigonometry, the estimated combined magnitude and angle can be calculated using just current for each coil set. The estimated combined field was verified using the same probe turned to the expected angle; this rough test yielded expected values, although more extensive verification can be done in the future with small Hall effect sensors.

B. AC Signal Coils

For magnetic testing, AC signals were generated for the device to detect using PCB RF coils. There are two functions an AC magnetic field generator must serve; the first is biomagnetic mimicking signals and the second is signals at the device's resonant frequencies. In order to assess the sensing capabilities in future studies, these AC coils must mimic biomagnetic signals and provide signals in the 1Hz to 1kHz range. Alternatively, in this study, the AC coils are used to deliver signals at device resonance, requiring powerful signals at around 70kHz and 6.5MHz. These direct resonant signals are analogous to WPT transmission signals.

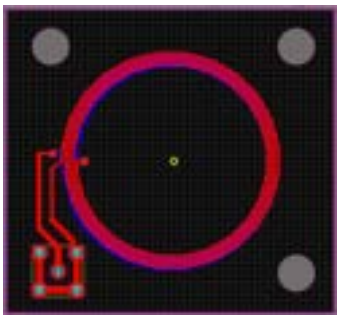

Fig. 8: PCB RF coil design for AC signals in Altium designer.

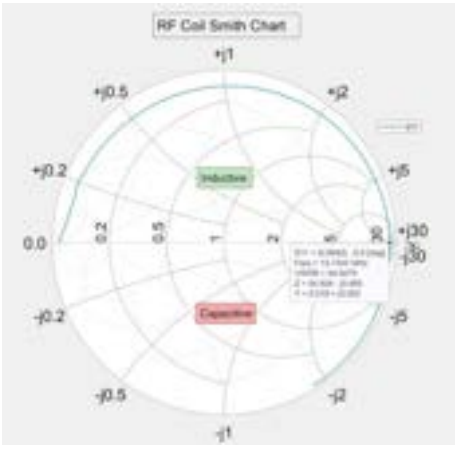

Fig. 9: Smith chart representation of operable ranges for AC coils.

Final coil design shown in Figure 8 is composed of a two layer rf coil with 4 turns per layer. The entire square board is 45mm wide, which is half the area of the previous model of AC coils used with these devices. Range of operation found using VNA is 1Hz -13MHz, as shown in the Smith chart in Figure 9. Beyond 13 MHz, the coil switches from acting as an inductor to acting as a capacitor and can no longer be used to generate signals. Overall, this coil design is smaller and more powerful than RF coils used in a previous study.

C. Overall Structure

To hold the DC bias coils, AC signal coils, and device, platform and device stages were designed. The platform shown in Figure 10 was designed to allow for testing in several different ways. The first is a plain parallel configuration with only one set of DC coils arranged parallel to the device beam. Secondly, a perpendicular platform attachment was made to allow for the addition of a perpendicular set of DC coils. Lastly, platform extenders were made to allow for more space in the center of the testing bed for future tests with large flux concentrators.

Device stages were designed to hold both the device and Transimpedance amplifier (TIA) circuit in the center of the fields. When directly detecting signals at resonance, the device output current must be amplified and converted to voltage using a TIA before going to a spectrum analyzer. The

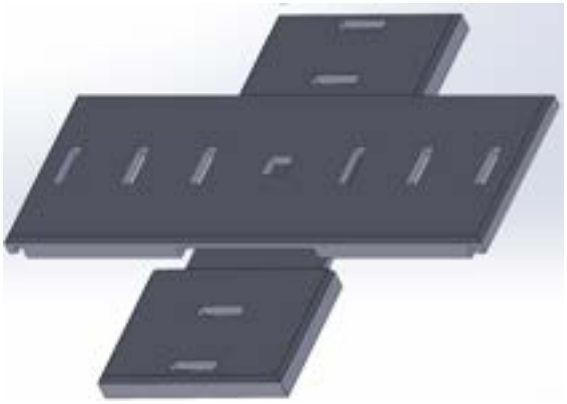

Fig. 10: Parallel platform and perpendicular attachment for testing with spaces for coils and device stage.

device stage design allows this TIA board and the device to sit steadily in the center of the field.

IV. Results

Figure 11 shows an example of electrical and magnetic data collected in one bias field. VNA output is shown as the electrical response on the left axis. The device output to a spectrum analyzer power at different signal frequencies is shown with the other lines on the right axis. Calculated SNR values for the magnetic response are shown. For subsequent data, only the frequency that yields the highest SNR is given; in this case the maximum SNR is 51.53 dBm occurring at an input signal of 69.9 kHz represents the maximum power out.

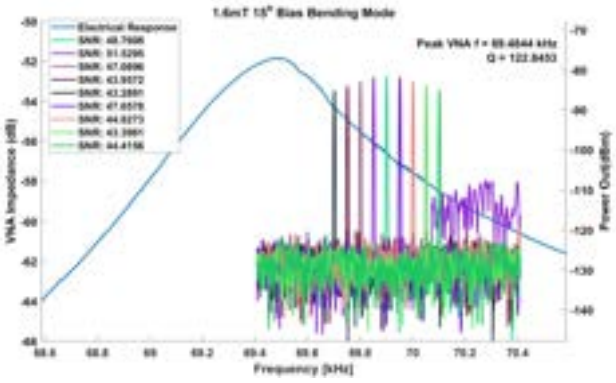

Fig. 11: Example electrical data from VNA (left axis) and magnetic data from several input signal frequencies (right axis) shown together.

A. Low Frequency Mode

Figure 12 gives the electrical (a) and magnetic (b) response for a device operating in the low frequency bending mode. This device is a medium ski design with an Iron Cobalt magnetostrictive layer. The Q-factor of the device increases with DC bias magnitude across all angles. Magnetically, the maximum power achieved by the device does not follow a clear pattern although an angled field shows improvement

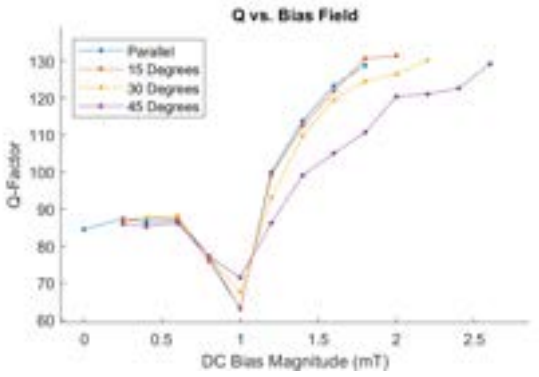

(a)

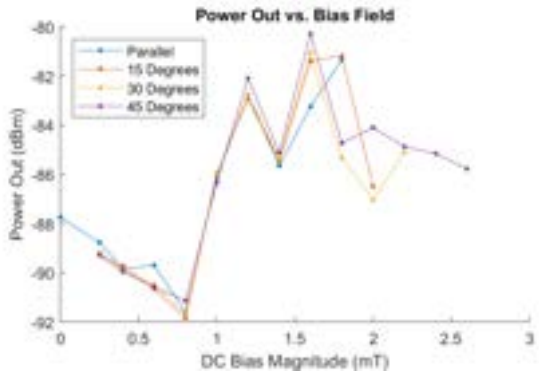

(b)

Fig. 12: Summary of bending mode in varied DC bias field shown in (a) Q-factors found from electrical testing and (b) maximum output power from magnetic testing.

at several bias magnitudes; most notably at 1.6mT of bias, there is an increase in performance as angle increases away from parallel.

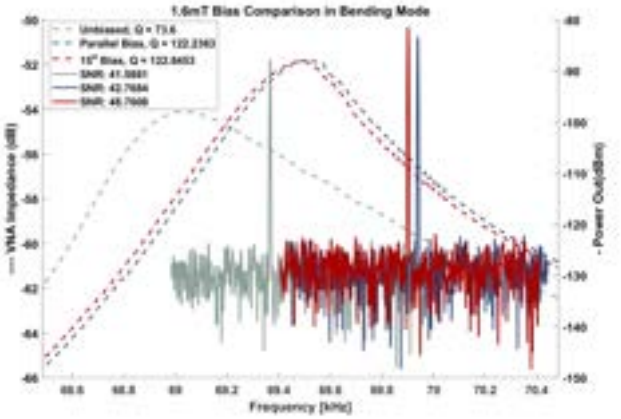

Fig. 13: Comparison of bending mode electrical and magnetic performance in unbiased, and 1.6 mT bias field at parallel and 15°.

A comparison of unbiased, parallel, and 15°bias is shown at this level in Figure 13. The improvement in Q-factor is clearly depicted visually with the narrowing of the VNA

peak. From unbiased to parallel 1.6mT bias, there is a 66% increase in the Q-factor. As was shown in Figure 12.a, there is no significant increase in Q-factor from parallel to 15o bias.

Conversely, the highest SNR improvements are linked to changes in bias angle rather than magnitude. Sensitivity increases by 1.18 dBm from unbiased to 1.6mT parallel bias, but increases 7.18 from unbiased to 1.6mT bias at 15°. This is a 2x sensitivity improvement achieved by just a slight bias rotation.

B. High Frequency Mode

Figure 14 gives the electrical (a) and magnetic (b) response for a device operating in the high frequency extensional mode. This device is a medium ski design with Hafnium-doped Iron Cobalt acting as the magnetostrictive layer. Similarly to the bending mode results, the Q-factor of the device increases with DC bias magnitude across all angles. Magnetically, the maximum power achieved by the device does not follow a clear pattern again although an angle field of 15o shows highest power across many of the field magnitudes.

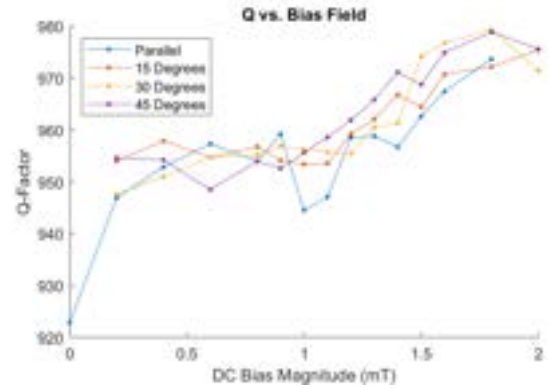

(a)

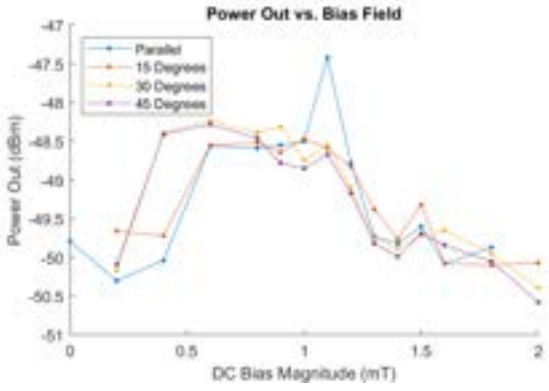

(b)

Fig. 14: Summary of extensional mode in varied DC bias field shown in (a) Q-factors found from electrical testing and (b) maximum output power from magnetic testing.

A comparison of unbiased, parallel 0.8mT, and 15o 0.8mT bias is shown at this level in Figure 15. The Q-factor improves from unbiased to biased again, although the difference

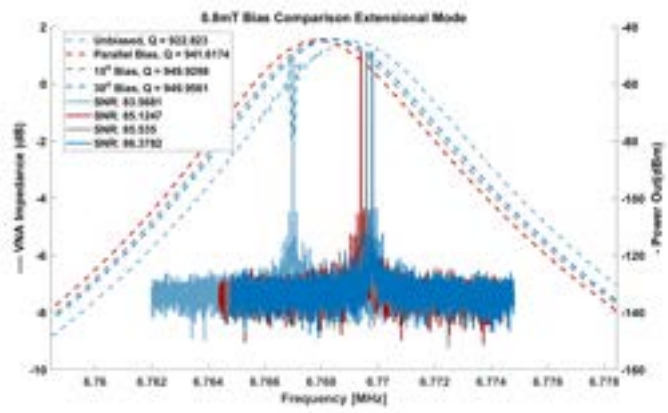

Fig. 15: Comparison of extensional mode electrical and magnetic performance in unbiased, and 0.8 mT bias field at parallel, 15°, and 30°

is not as substantial as was seen in the bending mode. An anomaly is noted in the unbiased VNA data, due to interference from an external field.

Extensional magnetic behavior is not as easily characterized as the bending behavior. There is a 1.56 dBm increase in sensitivity from unbiased to parallel bias. As angle increases, the sensitivity increases slightly. This trend is true at 0.8mT magnitude bias but not at every bias level, yielding inconclusive results.

V. Discussion

Overall, the electrical results from both modes of operation show that Q-factor increases to some extent with DC bias magnitude. The magnetic dipoles align more uniformly with the external field, causing the entire device to strain more easily with smaller electrical input than if they were randomly oriented. A similar phenomenon was expected for the magnetic response although these results are not seen here.

Figure 11 provides insight into some of the difficulties with collecting magnetic data. While VNA can clearly capture the Q-factor and electrical response, measuring the magnetic response is much less simple. This study was limited by the fact that magnetic data must be captured by sweeping input frequencies to find the maximum response in each bias field. This was done as precisely as possible, but a high resolution sweep of a wider range of frequencies was not feasible in the allotted time; thus, the magnetic data may have missed crucial ranges or trends that occur outside of the observed range. Further tests with more extensive sweeping for magnetic response are needed to capture the optimal bias field.

Additionally, low frequency data was taken using a low Q-factor device. To operate well in the bending mode, the neutral axis must not be within the piezoelectric layer as this causes charge to be lost. The only device available with an ideal neutral axis location was one with a low Q-factor as compared to other devices. Sensitivity improvements on a

low sensitivity device are difficult to attribute to one source, like bias, due the poor performance. A repeat study with other Iron Cobalt devices would provide more insight on bending mode behavior.

VI. Conclusion

This paper outlines a novel testing configuration and preliminary results. It is shown that ME devices may be optimized using an angle bias field although more in-depth testing is necessary. Provided is a structure and method by which to locate the optimal bias magnitude and angle. Outcomes show the potential that this testing method has for improving ME drives for important applications in biomedical devices.

There are several important future steps necessary to build on the work here. Firstly, angled bias has shown to improve magnetostriction in several materials that are not included here. Specifically, a study with Galfenol as opposed to Iron Cobalt could yield more interesting sensitivity improvement as it has shown higher performance in a 45°bias field [13]. Additionally, the inclusion of Hall effect sensors into the testing configuration would allow a more continuous characterization of the bias field as opposed to the static approach taken here. Lastly, once the optimal field for a given device and mode are identified, inclusion of permanent magnets into the device board would be a final step for device biasing. A small magnet would allow for a more compact sensor package for the applications outlined.

ACKNOWLEDGMENT

The author would like to thank Sydney Sofronici, Michael D'Agati, Dr. Troy Olsson, and the entire Olsson group at the University of Pennsylvania for everything they taught me and helped me accomplish so far this summer. Additional thanks to the National Science Foundation for funding the SUNFEST program with NSF REU grant no. 1950720, Dr. Sue-Ann Bidstrup Allen and Julia Falcon of the University of Pennsylvania for organizing the SUNFEST REU, and Biomedical Library's Printing Center for 3D printed structures.

References

[1] M. D'Agati, S. Sofronici, Yujia Huo, R. H. Olsson III, P. Finkel, K. Bussmann, T. Mion, M. Staruch, K. McLaughlin, B. Wheeler. "HighQ Factor, Multiferroic Resonant Magnetic Field Sensors and Limits on Strain Modulated Sensing Performance," to be published.

[2] Zuo, Siming, et al. "Modeling and Analysis of Magnetic Fields from Skeletal Muscle for Valuable Physiological Measurements." arXiv preprint arXiv:2104.02036 (2021).

[3] C. Wang, L. Sun, B. Lichtenwalter, B. Zerkle, B. Okada. (2016). Compact, ultra-low vibration, closed-cycle helium recycler for uninterrupted operation of MEG with SQUID magnetometers. Cryogenics. [Online]. 76, pp. 16-22. doi: https://doi.org/10.1016/j.cryogenics.2016.03.007.

[4] V. W. Leung et al., "A CMOS Distributed Sensor System for HighDensity Wireless Neural Implants for Brain-Machine Interfaces," ESSCIRC 2018 - IEEE 44th European Solid State Circuits Conference (ESSCIRC), Dresden, 2018, pp. 230-233.

[5] R. Jahns, R. Knochel, H. Greve, E. Woltermann, E. Lage and E. Quandt, "Magnetoelectric sensors for biomagnetic measurements," 2011 IEEE International Symposium on Medical Measurements and Applications, 2011, pp. 107-110, doi: 10.1109/MeMeA.2011.5966676.

[6] IEEE Standard for Safety Levels with Respect to Human Exposure to Radio Frequency Electromagnetic Fields, 3kHz to 300GHz", IEEE C95.1-1991

[7] V. Challa, J. Mur-Miranda, D. Arnold. (2012). "Wireless power transmission to an electromechanical receiver using low-frequency magnetic fields," Smart Materials and Structures, 21. doi: 10.1088/0964-1726/21/11/115017.

[8] R. Jahns, A. Piorra, E. Lage, C. Kirchhof, D. Meyners, J. L. Gugat, M. Krantz, M. Gerken, R. Knochel, E. Quandt. (2013). "Giant Magnetoelectric Effect in Thin-Film Composites." J. Am. Ceram. Soc., 96: 1673-1681. https://doi.org/10.1111/jace.12400

[9] D. Damjanovic, "Piezoelectricity," in Encyclopedia of Condensed Matter Physics, F. Bassani, G. L. Liedl and P. Wyder, Eds. Oxford: Elsevier, 2005, pp. 300-309.

[10] Zhou, Nanjia Blatchley, Charles Ibeh, Christopher. (2009). Design and construction of a novel rotary magnetostrictive motor. Journal of Applied Physics. 105. 07F113 - 07F113. 10.1063/1.3076896.

[11] H. Ogi et al, (2003), "Increase of Efficiency of Magnetostriction SHWave Electromagnetic Acoustic Transducer by Angled Bias Field: Piezomagnetic Theory and Measurement," Jpn. J. Appl. Phys. 42.

[12] K. Narita, J. Yamasaki and H. Fukunaga, "Measurement of saturation magnetostriction of a thin amorphous ribbon by means of small-angle magnetization rotation," in IEEE Transactions on Magnetics, vol. 16, no. 2, pp. 435-439, March 1980, doi: 10.1109/TMAG.1980.1060610.

[13] Patrick R. Downey and Alison B. Flatau "Bending behavior of iron-gallium (Galfenol) alloys for sensor applications", Proc. SPIE 5764, Smart Structures and Materials 2005: Smart Structures and Integrated Systems, (17 May 2005); https://doi.org/10.1117/12.600107